

Supplementary Information

Band Bending Reversal and Enhanced Electron Mobility at Film

Surface Achieving through a Selective Polishing Strategy in Tin-Lead

Perovskite Solar Cells

Yuyang Hu[†], Haobo Yuan[†], Wenxiao Zhang,^{*} Xuemin Guo, Nannan Sun, Wen Li, Zhengbo Cui, Xiaodong Li,^{*} and Junfeng Fang^{*}

School of Physics and Electronic Science, Engineering Research Center of Nanophotonics & Advanced Instrument, Ministry of Education, East China Normal University, Shanghai 200062, China.

E-mail: wxzhang@phy.ecnu.edu.cn, xdli@phy.ecnu.edu.cn, jffang@phy.ecnu.edu.cn.

Experimental

Materials

NiO_x nanoparticles (NPs) powder, Tin (II) iodine (SnI₂, 99.999%), CH(NH₂)₂I (FAI) (99.9%), [6,6]-phenyl-C₆₁-butyric acid methyl ester (PC₆₀BM, 99.9%) were purchased from Advanced Election Technology CO. Ltd. CH₃NH₃I (MAI) (≥99.5%), guanidinium thiocyanate (GASCN) (≥99.5%), PbI₂ (≥99.99%), lead bromine (PbBr₂, 99.9%), cesium iodine (CsI, 99.999%), C₆₀ (>99%) and 1,3,5-Tris(1-phenyl-1H-benzimidazol-2-yl)benzene (TPBI, >99%) were offered by the Xi'an Polymer Light Technology. Tin (II) fluoride (SnF₂, >99%), ethanol (≥99.9%), pyrophosphoric acid (PP, ≥94%), Chlorobenzene (anhydrous, 99.8%), 2-propanol (IPA, 99.5%), dimethylformamide (DMF, 99.8%), the dimethyl sulfoxide (DMSO, ≥99.9%) solvent and ethylenediamine (EDA, ≥99%) solvent were purchased from Sigma-Aldrich. Poly [3-(4-carboxylbutyl) thiophene] (P3CT) was obtained from Rieke, America. Lead powder (Pb, 99.95%) and Cesium hydroxide monohydrate (CsOH•H₂O, 99.9%) were achieved from Aladdin. [4-(3,6-dimethyl-9H-carbazol-9-yl)butyl]phosphonate acid (Me-4PACz, >99.0%) and 1,3-propane-diammonium iodide (PDAI₂) were bought from TCI company. Lead(II) Thiocyanate (Pb(SCN)₂, ≥98%) was purchased from Macklin. Atomic layer deposition (ALD) precursor of tetrakis(dimethylamino) tin (iv) (99.99%-Sn, 50-1,815 tin) was bought from Langchen Micro (Shanghai). All solutions were filtered with a 0.2 μm PTFE filter before use. All materials in this literature were utilized as received from commercial without further purification.

Device fabrication

Single-junction devices

FTO glass substrates were ultrasonically cleaned by detergent, DI water, acetone, and isopropanol for 20 min respectively followed by UV-zone for 20 min to increase wettability. P3CT-Cs solution was synthesized by dissolving 10 mg P3CT and 9 mg CsOH•H₂O in methanol. The 0.5 mg•ml⁻¹ P3CT-Cs solution was spin-coated on FTO substrates at 3000 rpm for 30 s. Then, the P3CT-Cs film was annealed at 100 °C in air for 10 min. After that, the substrates were immediately transferred to N₂ glovebox for the deposition of perovskite film. For the Sn-Pb mixed perovskite precursor, Sn- and Pb-based precursor were prepared separately and mixed before use. For tin-based precursor, 0.76 mmol FAI, 0.75 mmol SnI₂, 0.075 mmol SnF₂, and 0.03 mmol GASCN were dissolved in 500 μl DMF and DMSO (v/v = 3:1) solvent. After adding 30 mg lead powder, the tin-based precursor was stirred at room temperature overnight over 10 h. For lead-based precursor, 0.15 mmol CsI, 0.15 mmol FAI, 0.45 mmol MAI and 0.75 mmol PbI₂ were dissolved in 500 μl DMF and DMSO (v/v=3:1) solvent before using and stirred for 30 min. The tin- and lead-based precursor was mixed in equal volume and filtrated before spin-coating perovskite film. The Sn-Pb mixed perovskite film was spin-coated on P3CT-Cs layer at 1000 rpm for 10 s with an acceleration speed of 200 and 4000 rpm for 80 s. 400 μl chlorobenzene was dropped on the substrate 5-10 s before the end of the second program. Afterwards, the perovskite films were annealed at 100 °C for 10 min. Next, the perovskite films were treated with PP of different concentrations (0-0.6 mg/ml) in isopropanol (IPA) at 4000 rpm for 30 s with hot post-treatment at 100 °C for 3 min. Moreover, 0.1 mM EDA in

isopropanol (IPA) was deposited on the fabricated perovskite films with PP at 5000 rpm for 20 s with annealing at 100 °C for 5 min.¹ The PCBM (10 mg/ml in CB) layers were coated on the cooled films via 2000 rpm for 30 s. Eventually, the substrate was removed into a vacuum chamber. 30 nm C₆₀, 6 nm TPBI, and 100 nm Ag electrode were thermally evaporated under high vacuum ($< 5 \times 10^{-4}$ Torr). The device area is 0.09 cm² with an overlap of Ag and FTO.

All-perovskite tandem devices

ITO substrates were washed with the same procedures as FTO in the single-junction devices. NiO_x NPs were decentralized in DI H₂O to a concentration of 10 mg/ml and then were spin-coated on cleaned ITO substrates at 3000 rpm for 30 s, annealing at 100 °C for 10 min in air. Then the substrates were transferred into a glovebox to self-assemble the Me-4PACz (0.3 mg/ml in ethanol) at 4000 rpm for 30 s, and annealed at 100 °C for 10 min. For the wide band-gap perovskite precursor solutions (1.2 M, FA_{0.8}Cs_{0.2}PbI_{1.8}Br_{1.2}) precursor, 0.96 mmol FAI+0.24 mmol CsI+ 0.48 mmol PbI₂+0.72 mmol PbBr₂+0.01 mmol Pb(SCN)₂ were dissolved in 1 ml mixed solvent DMF/DMSO with volume ratio of 4:1. The precursors were stirred for 1 h to dissolve all chemicals and further filtered with 0.22 mm poly (tetrafluoroethylene) (PTFE) membrane before using. Then wide-band-gap (WBG) perovskite films were deposited on the substrates at 2000 rpm for 10 s with an acceleration speed of 200 and 4000 rpm for 20 s. At the second stage, 60 μl CB antisolvent was dropped on the wet films at 10 nd s immediately followed by annealing at 60 °C for 3 min and 100 °C for 12 min. Then PDAI₂ (1 mg/ml in 2-propanol) was dynamically coated on the WBG perovskite surface at 4000 r 30 s, followed by annealing at 100 °C for 5 min. Subsequently, the substrates were transferred into an evaporation chamber to deposit 30 nm C₆₀. The deposition of ALD-SnO₂ was performed using tetrakis (dimethylamino) tin (IV) and deionized water as precursors. 25 nm ALD SnO₂ film and 1 nm Au were deposited on the substrates sequentially. Then 3mg/ml P3CT-Cs in methanol solution for tandems was spin-coated at 4000 rpm for 30 s in air, then further dried at 100 °C for 10 min. After that, the preparation of the Sn-Pb LBG (low-band-gap) perovskite films was the same as the single-junction devices.

Characterization

Scanning electron microscope (SEM) images were recorded by leveraging a field-emission scanning electron Microscopy (Zeiss GeminiSEM450). Energy-dispersive X-ray spectroscopy (EDS) was recorded by SEM (FEI Quanta FEG 250) with an accelerating voltage of 20 kV. Fourier transform infrared (FTIR) Spectrometer was measured using Nicolet iS50, thermo. X-ray diffraction (XRD) spectra was conducted in an Empyrean Micro diffractometer with Cu K α radiation. The ToF-SIMS measurements (PHI nano TOF II Time-of-Flight SIMS) were carried out with the pulsed primary ions from a Cs⁺ (1 keV, 60 nA sputter current) ion gun for the sputtering and a Bi₃⁺⁺ pulsed primary ion beam for the analysis (30 keV, 0.75 pA pulsed current). The sputter area of 200×200 μm² with 50×50 μm² analysis area was centered inside the Argon raster area, and the sputter rate was calibrated with the GaN substrate on each batch of samples. On account of the extremely high sensitivity of TOF-SIMS and the inevitable roughness of each layer, all the ion intensity curves usually extended their regions and overlapped at the interfaces. The surface Kelvin Probe Force Microscopy (KPFM) was analyzed with Bruker Multimode 8 atomic force microscope using a silicon probe coated with 0.01-

0.025 Ohm-cm Antimony(n) with a force constant of 3 N/m and a tip radius of 30 nm. The cross-sectional KPFM measurements were carried out by Dimension Icon SPM (Bruker). A Pt/Ir-coated tip with a resonant frequency of 75 kHz, and a scanning frequency of 1Hz to measure the topography and potential images in air. X-ray photoelectron spectroscopy (XPS) and ultraviolet photoelectron spectroscopy (UPS) measurements were carried out using the Kratos AXIS ULTRA DALD XPS/UPS system. The steady-state and time-resolved PL spectra were measured utilizing the FLS980E Fluorescence Spectrophotometer (excited by 532 nm, United Kingdom) at FOMAD (Family of Master and Doctor) Corp, China. The PL Mapping was measured under excitation of a 510 nm pulsed laser with a power density of $15 \mu\text{J}\cdot\text{cm}^{-2}$, based on a FLS920 (Edinburgh Instruments) fluorescence spectrometer. The Titanium: Sapphire femtosecond laser (Astrella, Coherent Inc) generates femtosecond pulsed light with a central wavelength of 800 nm, a repetition rate of 1 kHz, and a pulse width of 100 fs. This 800 nm pulsed light is split into two parts by a beam splitter. One part enters the optical parametric amplifier (OPerA Solo, Coherent Inc) to produce the pump light at 600 nm. The other part passes through a delay line (Delayline) and enters the transient absorption spectrometer (Helios, Ultrafast system), where it is focused on a sapphire nonlinear to generate a supercontinuum probe light. The probe light, after being focused by an off-axis parabolic mirror, is directed onto the sample. The pump light, after being chopped to 500 Hz by a chopper, is adjusted by a half-wave plate to ensure that the pump and probe lights are focused onto the sample at an angle of 54.7° . During testing, the sample is clamped on a sample stage that can move two-dimensionally in the direction perpendicular to the beam to reduce damage to the sample from the pump light). The probe light absorbed by the sample carries information about the particle's excited state and ground state and is ultimately incident on the optical fiber probe head. By using a time delay line to change the delay of the probe light relative to the pump light reaching the sample, spectral information of the sample particles at different time delays after excitation can be obtained. ^{119}Sn nuclear magnetic resonance (NMR) spectra were measured with an AVANCE III (500MHz). UV-vis absorption spectra was measured using PE Lambda750 S (PerkinElmer). Photocurrent density-voltage (J - V) curves (Keithley 2400 Source Meter) were measured under one sun illumination (AM1.5G, $100 \text{ mW}\cdot\text{cm}^{-2}$) using the solar simulator (Enlitech, SS-F5-3A). The light source is a 450-W xenon lamp calibrated by a standard Si reference solar cell (Enli/SRC2020, SRC-00201). The J - V curves were evaluated from 1.0 V to -0.2 V with a dwell time of 5 ms. The light source is a 45-W xenon lamp calibrated by a standard Si reference solar cell (Enli/SRC2020, SRC-00201). The EQE measurement was performed in ambient air using a QE system (SOFN Instruments Co., Ltd) with monochromatic light focused on a device pixel. For tandem PSCs, 530 and 940 lamps were applied to collect the EQE of the bottom and top subcells, respectively. The air stability of unpacked Sn-Pb PSCs was performed at the controlled RH of 30-40% dark box and their photovoltaic performances were tested regularly. The 65°C thermal stability of PSCs was measured at a 65°C hotplate in the N_2 glovebox.

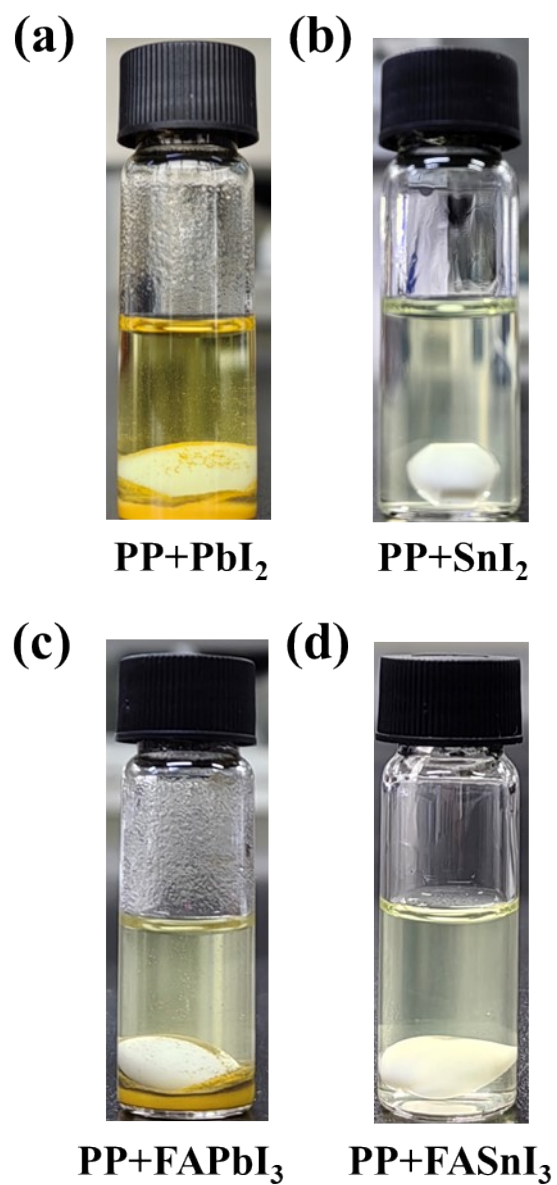


Fig. S1. Photographs of (a) PP+PbI₂ (b) PP+SnI₂ (c) PP+FAPbI₃ (d) PP+FASnI₃ in IPA.

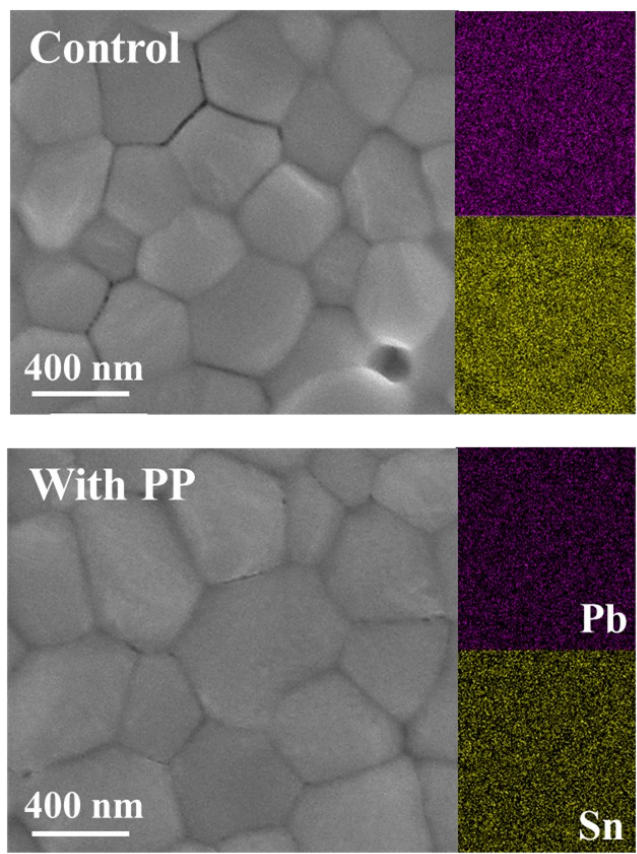


Fig. S2. Scanning electron microscope (SEM) and EDS images of the control and PP-polished film.

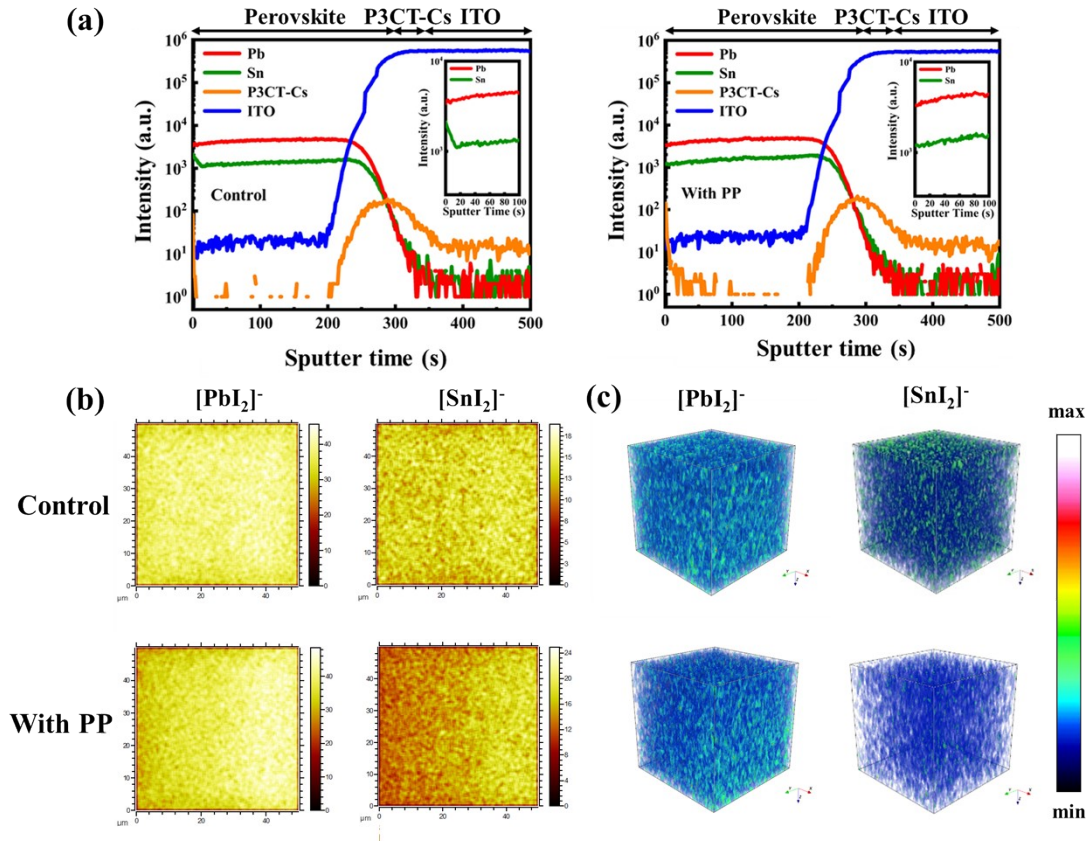


Fig. S3. (a) TOF-SIMS depth profile of the control and PP polished Sn-Pb perovskite film (Inset shows the enlarged view of the top region). (b) TOF-SIMS 2D images comparing molecular fragments ($[PbI_2]^-$ and $[SnI_2]^-$) of untreated and PP-modified perovskite films measured in negative polarity. (c) TOF-SIMS reconstructed 3D tomography showing the spatial distribution of notable molecular ions $[PbI_2]^-$ and $[SnI_2]^-$ over $50 \times 50 \mu m$ raster size in the XY direction and 1200 s etching time in the Z direction for untreated and iodide-treated samples.

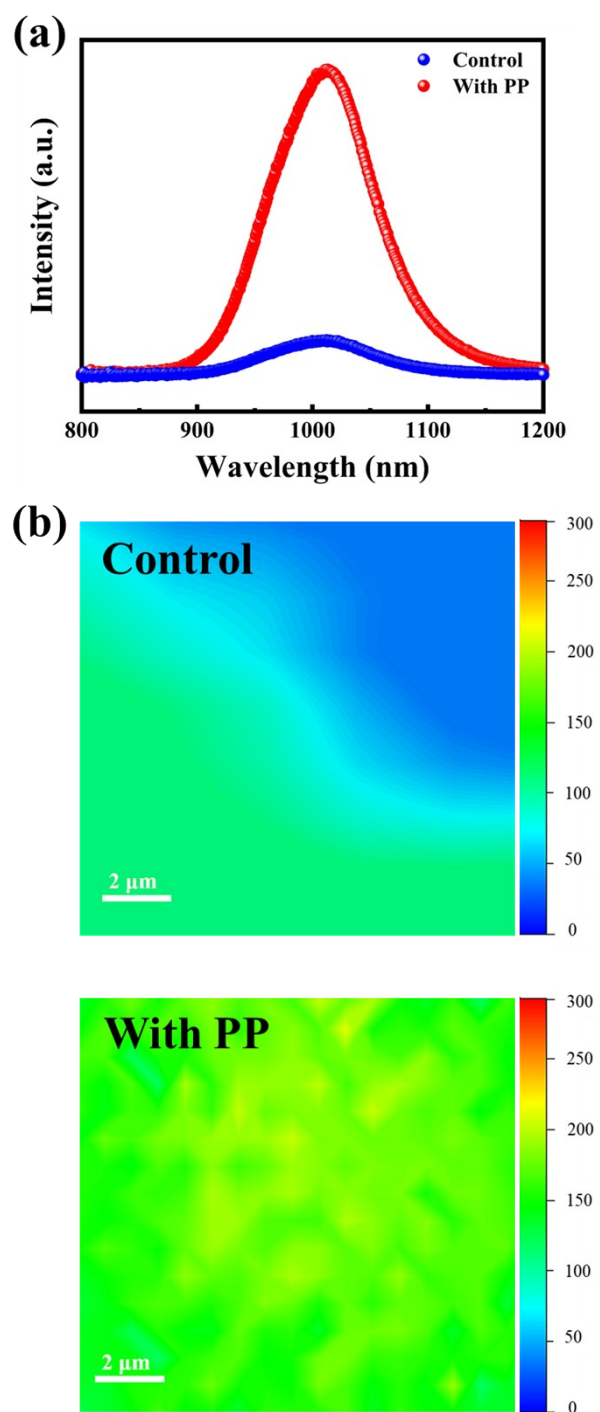


Fig. S4. (a) PL and (b) Micro-PL mapping of the control perovskite and perovskite with PP.

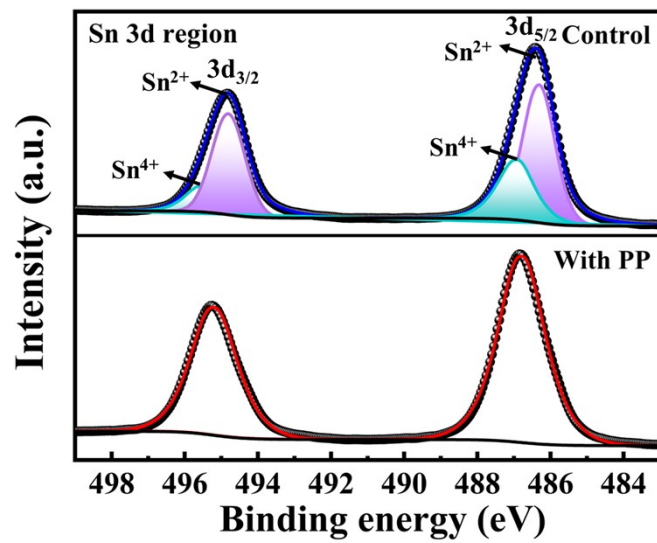


Fig. S5. XPS spectra of Sn 3d region in the control and PP-treated perovskite films.

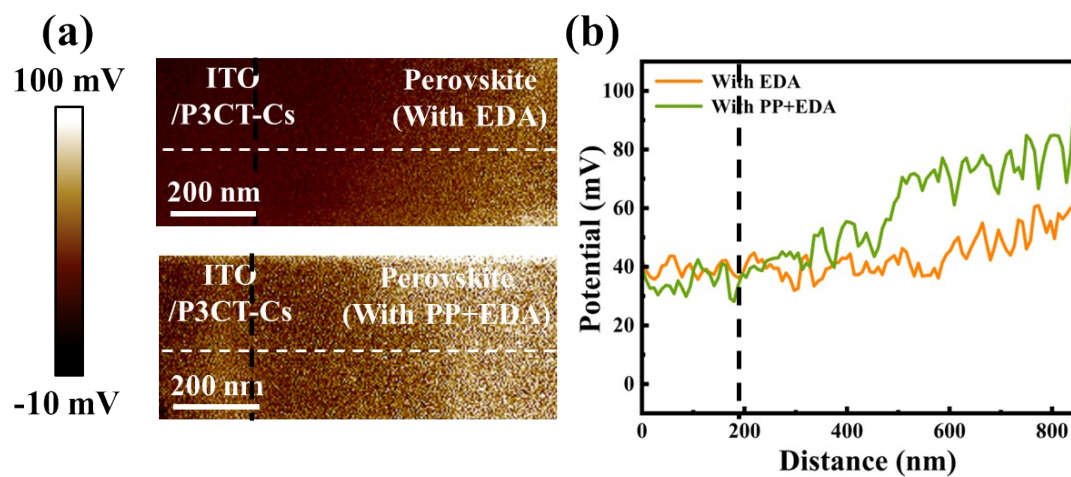


Fig. S6. Cross-sectional potential mapping of the films with EDA and with PP+EDA by KPFM.

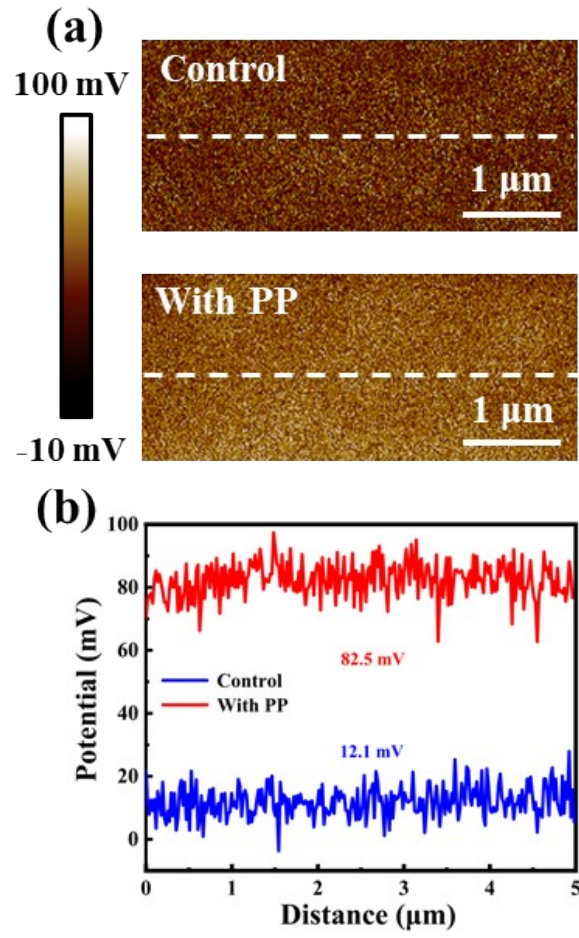


Fig. S7. (a) Surface potential mapping of the control and perovskite films with PP. (b) Line profiles of cross-sectional KPFM in the control and PP-modified perovskite films.

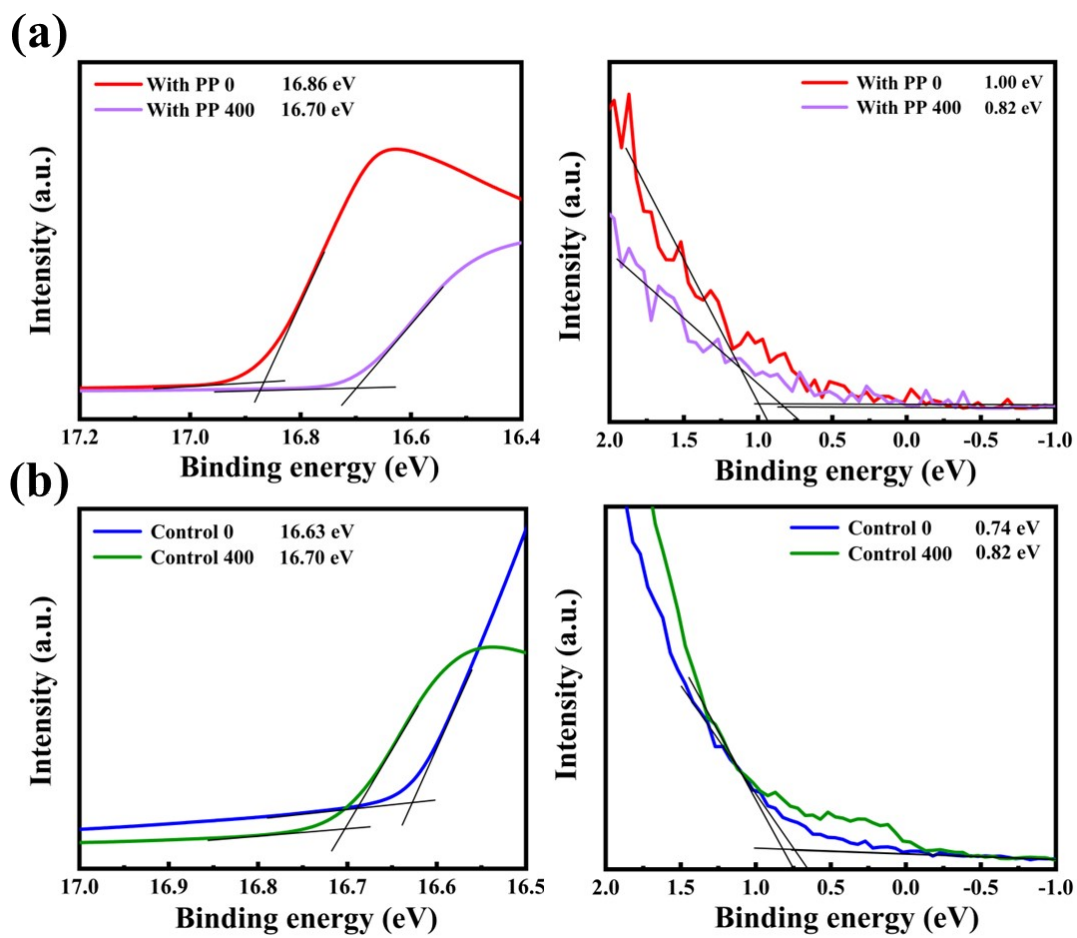


Fig. S8. UPS spectra of (a) the control and (b) PP-treated perovskite film at the surface and in the etching depth of 400 nm.

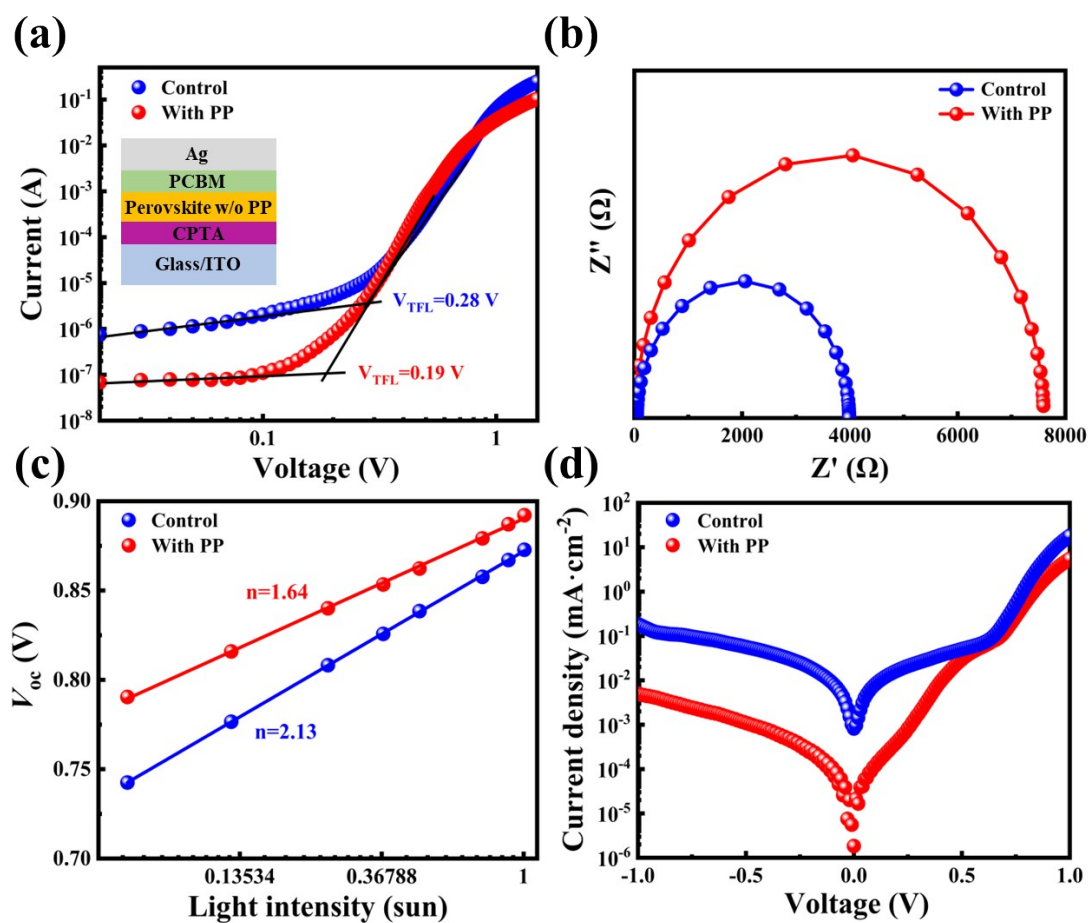


Fig. S9. (a) Space-charge-limited current measurement (SCLC) for electron-only devices (glass/ITO/CPTA/perovskite/PCBM/Ag) based on different perovskite layers. (b) The Nyquist plots based on the control and PP-modified perovskite. (The inset shows the equivalent circuit in PSCs.) (c) Light dependence of V_{oc} of devices based on the perovskite layer with and without PP and (d) J - V curves under dark conditions.

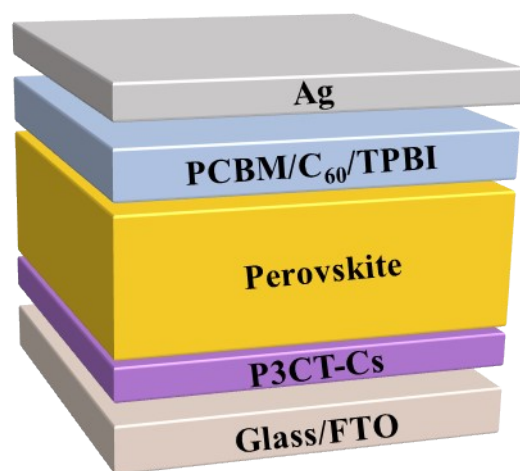


Fig. S10. Schematic of the device architecture for Sn-Pb PSCs.

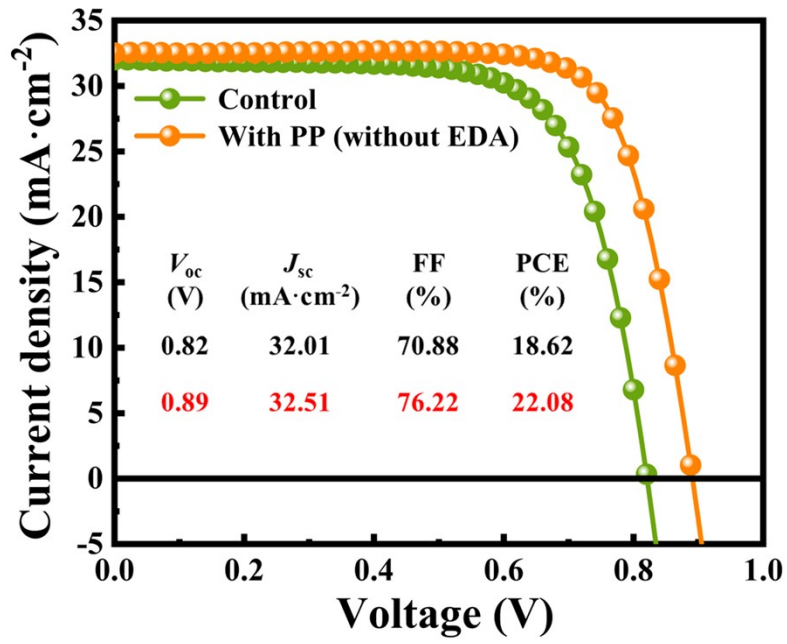


Fig. S11. *J-V* curves of the control devices and the devices with PP but without EDA treatment.

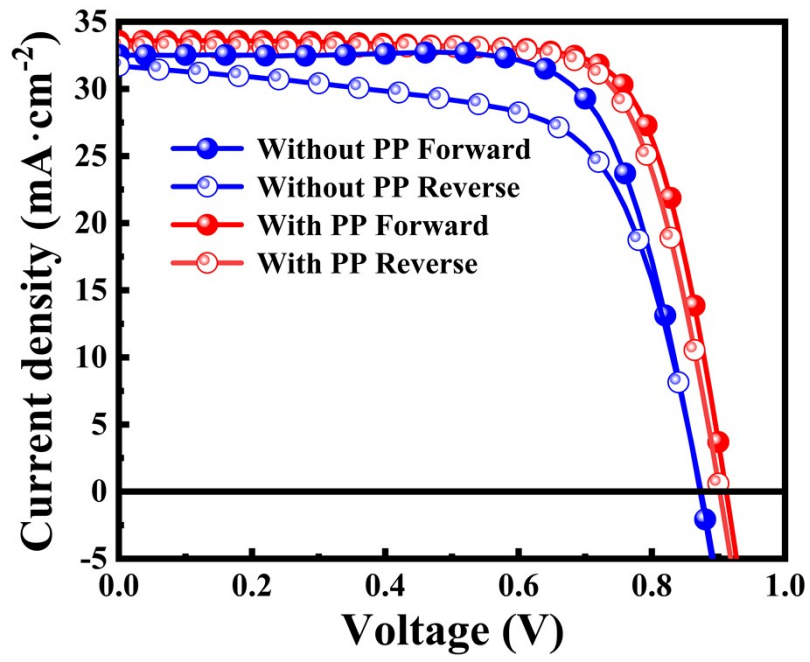


Fig. S12. *J*-*V* curves of mask devices with and without PP measured by forward and reverse scans. (mask area: 0.0886 cm²).

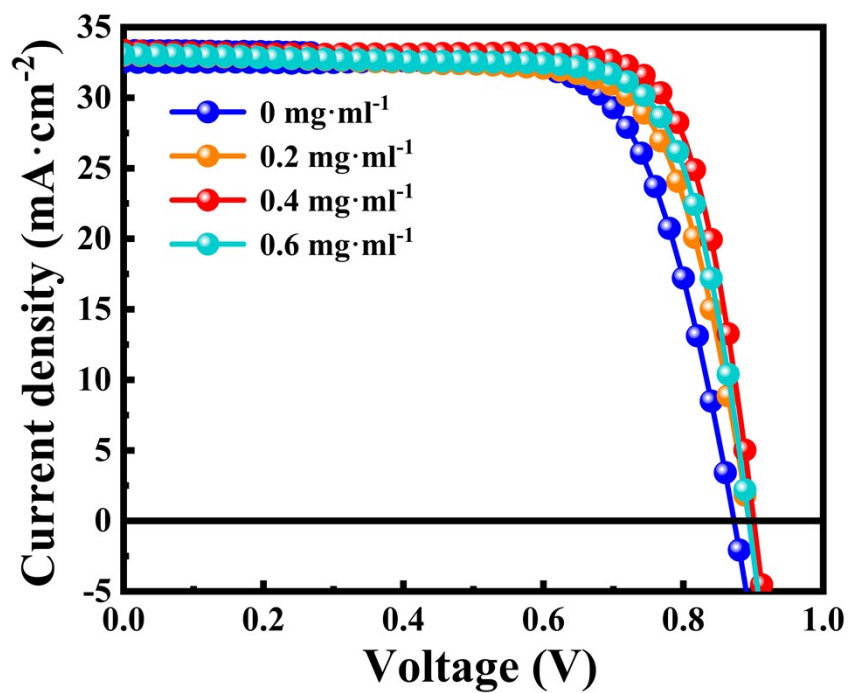


Fig. S13. *J-V* curves of PSCs with different concentrations of PP.

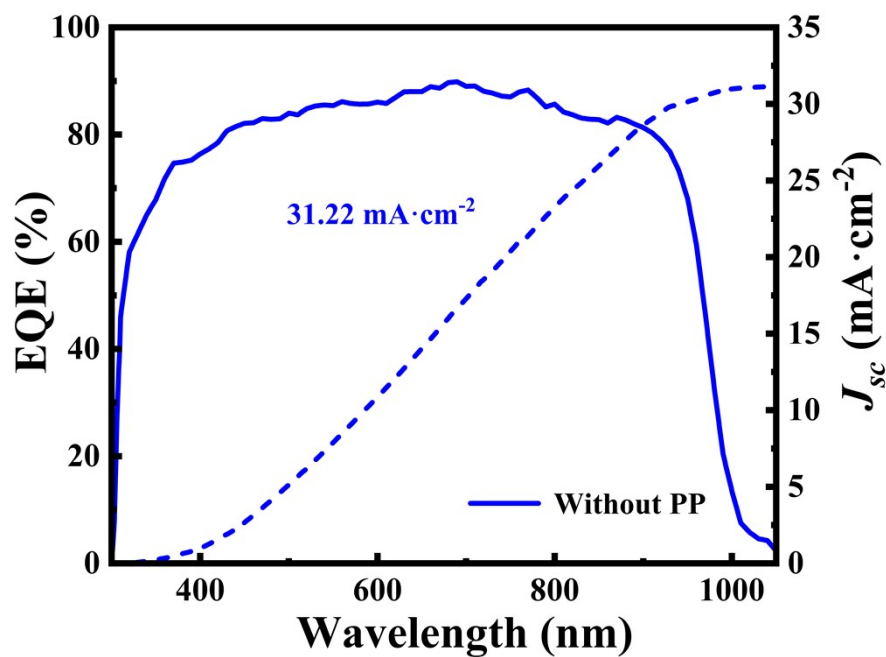


Fig. S14. External quantum efficiency (EQE) and integrated current density (J_{sc}) recorded for PSCs without PP treatment.

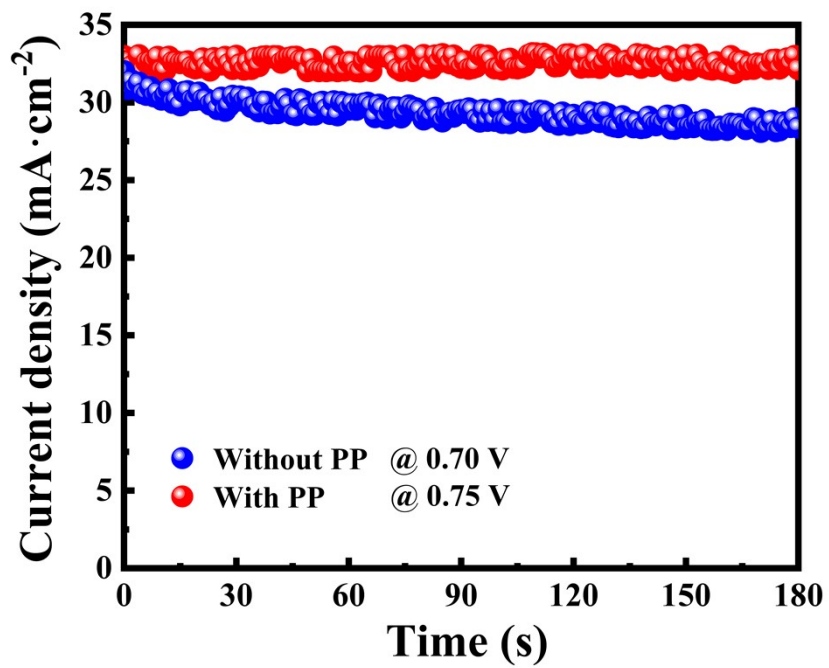


Fig. S15. Maximum power point (MPP) measurement of PSCs with and without PP.

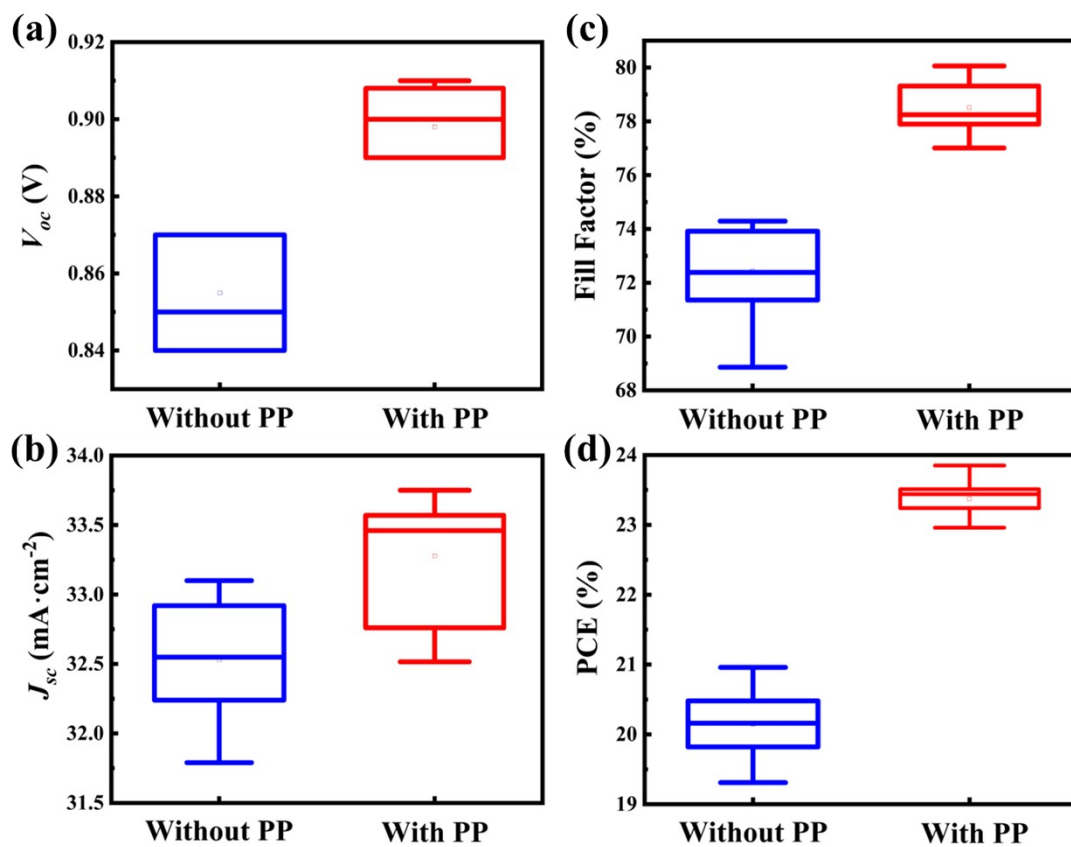


Fig. S16. The statistical distribution of 20 randomly selected devices. (a) V_{oc} (b) J_{sc} (c) FF and (d) PCE.

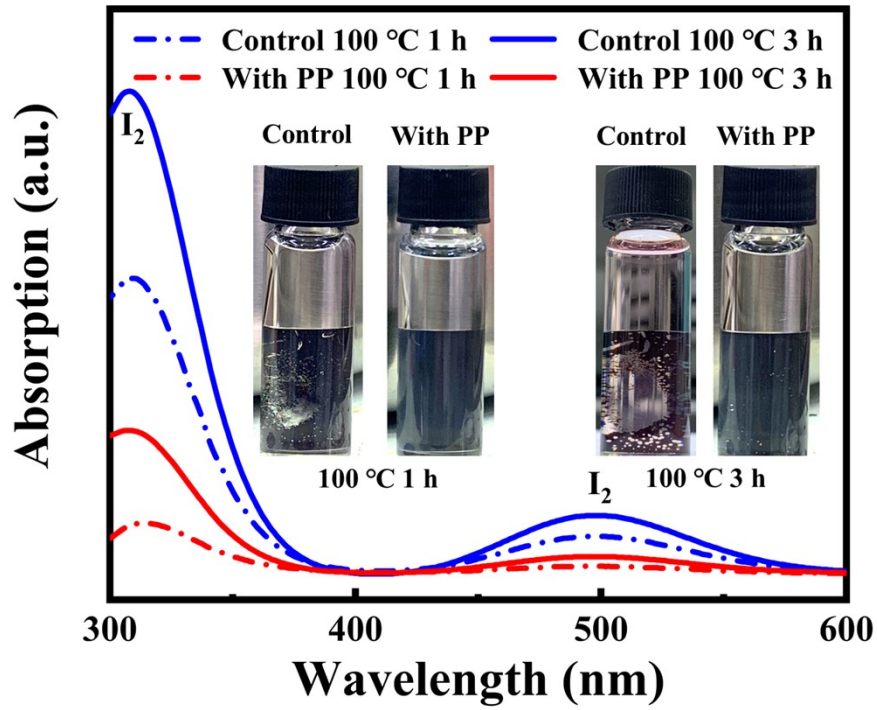


Fig. S17. Ultraviolet-visible (UV-Vis) absorption spectra of the toluene in which the control and PP-polished perovskite film aged in N_2 at $100\text{ }^\circ\text{C}$ (Inset shows the photographs of the control and PP-treated perovskite films immersed in the toluene solution under $100\text{ }^\circ\text{C}$ for 1 h and 3 h).

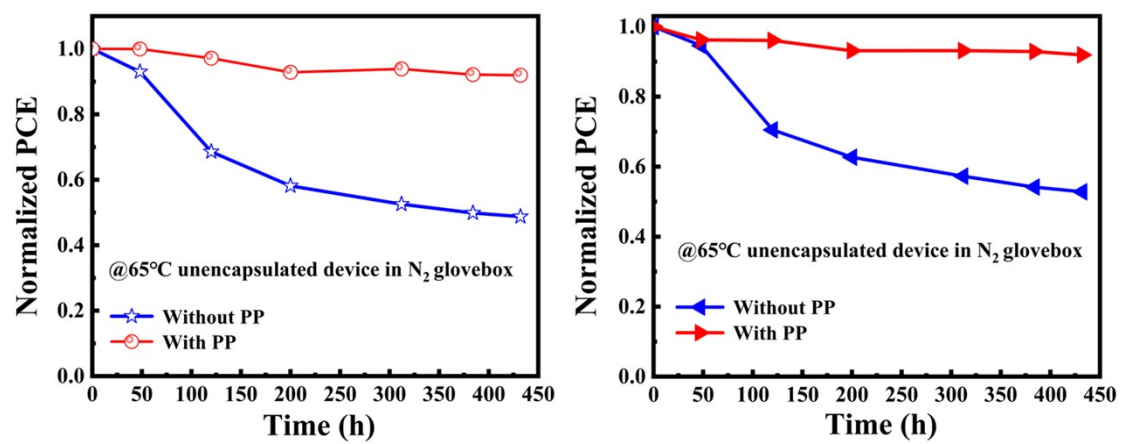


Fig. S18. The other two thermal stability tests of devices randomly selected with and without PP treatment under a thermal stress at 65 °C.

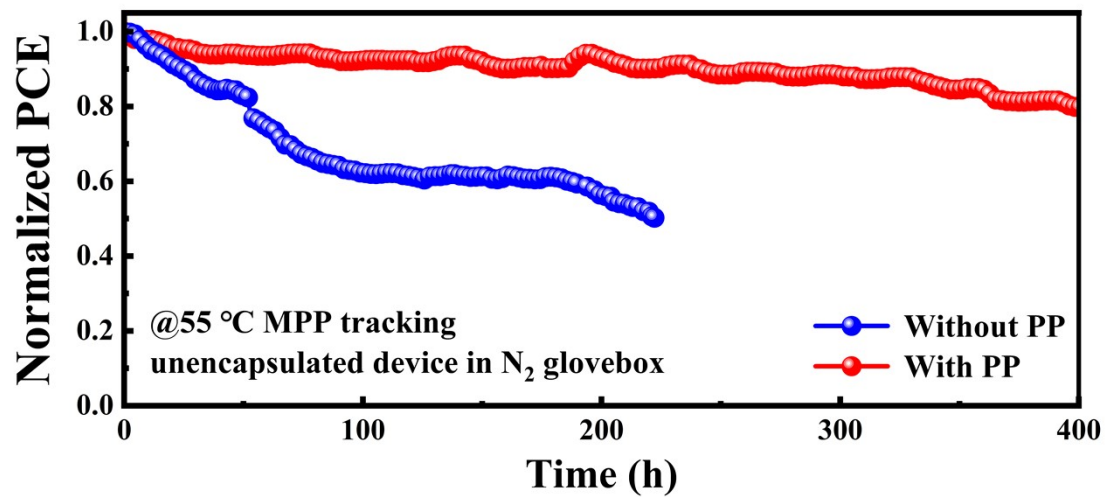


Fig. S19. Operational stability of PSCs during MPP tracking at 55 °C.

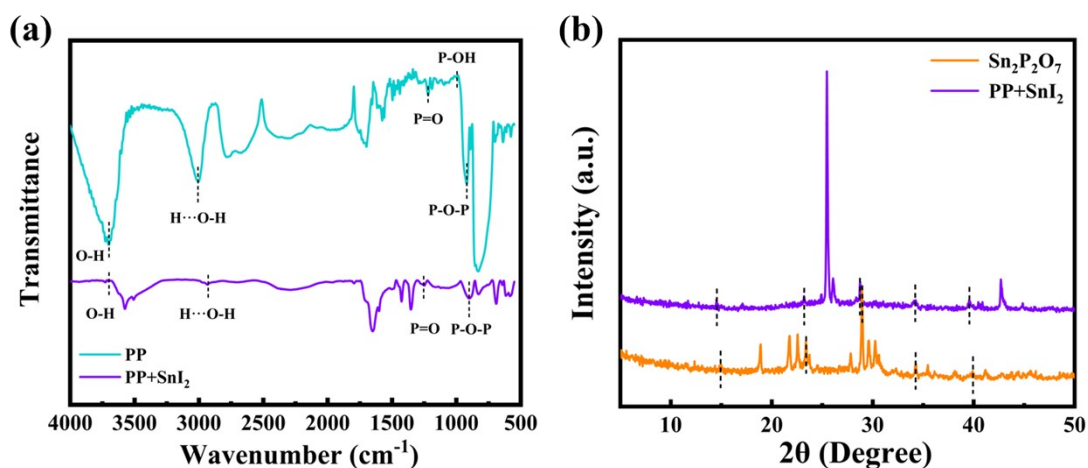


Fig. S20. (a) FTIR spectra of PP and PP+SnI₂. (b) XRD patterns of Sn₂P₂O₇ and PP+SnI₂.

PP interacts with SnI₂ through the formation of a P-O···Sn coordination bond. In Fourier transform infrared (FTIR) spectroscopy (Fig. S20a ESI[†]), the P-OH signal disappears after interacting with SnI₂ and produces stannous pyrophosphate as evidenced by X-ray Diffraction (XRD) patterns (Fig. S20b ESI[†]). These observations suggest that PP interacting with SnI₂ through the formation of multidentate complex.

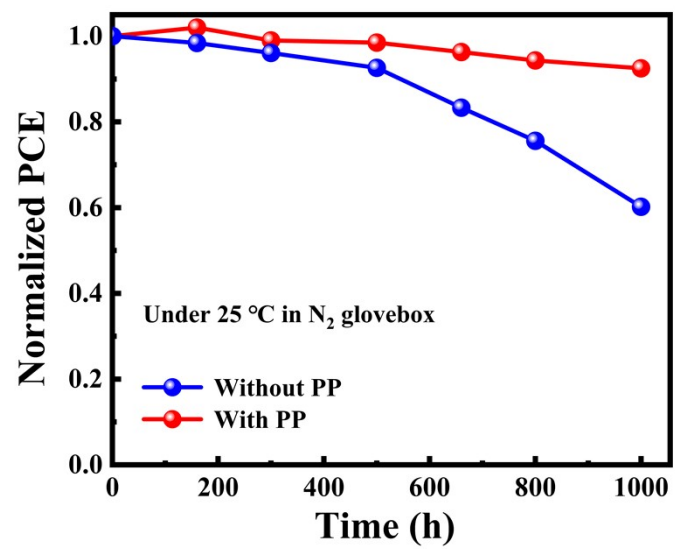


Fig. S21. Stability of devices with and without PP treatment storing in N₂.

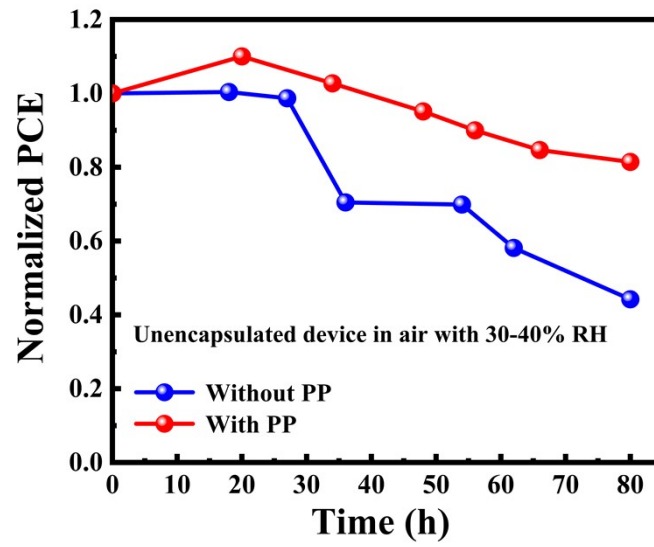


Fig. S22. Stability of devices with and without PP treatment with 30-40% relative humidity (RH).

Table S1 EDS results of Pb and Sn element content of the control and PP-polished perovskite films.

Name	Atomic% (Control)	Atomic% (PP)
Pb	43	50
Sn	57	50

Table S2 XPS spectra of Sn and Pb element content of the control and PP-treated perovskite films.

Name	Peak BE	Area (P) CPS.eV	FWHM eV	Atomic %
Control				
Sn 3d	486.77	3066257.03	2.46	70.76
Pb 4f	137.87	1434604.60	2.27	29.24
With PP				
Sn 3d	487.00	1604488.46	2.57	45.92
Pb 4f	137.96	1715155.92	2.44	54.08

Table S3 Fitted parameters of time-resolved PL decay curves for the control and PP-treated

Sample	τ_1 (ns)	τ_2 (ns)	A_1	A_2	τ_{average} (μs)
Control	2577.7	10383.3	0.84	0.26	6.9
With PP	8459.9	8460.0	0.49	0.48	8.5

film.

Table S4 Fitted parameters of fs-TA decay curves for the control and PP-treated film.

Sample	τ_1 (ps)	τ_2 (ps)	τ_3 (ps)
Control	56.54	529.0	2280.0
With PP	45.12	474.2	903.1

Table S5 EIS fitting results of the control and PP-polished devices.

Sample	R_s (Ω)	R_{rec} (Ω)
Control	48	3936
With PP	18	7578

Table S6 Summary of photovoltaic performance of the Sn-Pb devices with different concentrations of PP.

PP Concentration (mg/ml)	V_{oc} (V)	FF (%)	J_{sc} (mA·cm ⁻²)	PCE (%)
Control	0.87	74.01	32.56	20.98
0.2 mg/ml	0.91	76.86	32.53	22.75
0.4 mg/ml	0.91	79.31	33.05	23.85
0.6 mg/ml	0.90	78.39	32.28	22.77

No	V_{oc} (V)	FF (%)	J_{sc} (mA·cm ⁻²)	PCE (%)
1	0.91	79.31	33.05	23.85
2	0.90	77.75	33.75	23.62
3	0.91	78.23	33.16	23.61
4	0.89	78.74	33.57	23.53
5	0.89	78.92	33.50	23.53
6	0.89	78.15	33.80	23.51
7	0.91	77.81	33.19	23.50
8	0.91	79.31	32.55	23.49
9	0.89	78.84	33.46	23.48
10	0.90	78.13	33.38	23.47
11	0.90	78.09	33.35	23.44
12	0.89	79.56	33.10	23.44
13	0.89	80.05	32.77	23.35
14	0.90	77.17	33.60	23.34
15	0.89	78.26	33.50	23.33
16	0.89	79.71	32.76	23.24
17	0.89	80.06	32.39	23.08
18	0.91	77.01	32.83	23.01
19	0.90	77.16	33.06	22.96
20	0.89	77.98	33.22	23.06
Average	0.8975±0.00851	78.519±0.93848	33.20±0.39136	23.40±0.22624

Table S7 Photovoltaic parameters of 20 randomly selected devices with PP treatment.

Table S8 Photovoltaic parameters of 20 randomly selected devices without PP treatment.

No	V_{oc} (V)	FF (%)	J_{sc} (mA·cm ⁻²)	PCE (%)
1	0.87	74.01	32.56	20.96
2	0.87	73.92	32.36	20.81
3	0.85	73.26	33.10	20.61
4	0.85	74.29	32.55	20.55
5	0.86	72.50	32.86	20.49
6	0.84	74.03	32.94	20.48
7	0.84	73.48	33.02	20.38
8	0.87	70.96	33.01	20.38
9	0.84	73.28	32.92	20.26
10	0.84	73.91	32.30	20.16
11	0.87	71.76	32.26	20.14
12	0.84	74.19	32.20	20.06
13	0.87	72.27	31.88	20.04
14	0.85	72.10	32.61	19.99
15	0.85	70.94	32.99	19.82
16	0.85	72.11	32.29	19.79
17	0.86	69.51	32.87	19.65
18	0.84	72.23	32.18	19.52
19	0.86	70.94	31.79	19.39
20	0.87	68.86	32.24	19.31
Average	0.8545±0.01234	72.4275±1.57515	32.5465±0.40078	20.1395±0.45987

References

1. W. Zhang, H. Yuan, X. Li, X. Guo, C. Lu, A. Liu, H. Yang, L. Xu, X. Shi, Z. Fang, H. Yang, Y. Cheng and J. Fang. *Adv Mater.*, 2023, **35**, 2303674.